

A deep mantle origin for the primitive signature of ocean island basalt

Frédéric Deschamps^{1*}, Edouard Kaminski² and Paul J. Tackley¹

Seismological observations have identified large-scale compositional heterogeneities in the Earth's deep mantle^{1–5}. These heterogeneities may represent reservoirs of primitive material that differentiated early in Earth's history^{6–8}. The volcanic rocks that make up ocean islands are thought to be sourced, in part, from these deep reservoirs, with the primitive material transported to the surface via mantle plumes. Geochemical signatures within the erupted ocean island basalts further support the idea that the regions of heterogeneity are composed of primitive, undegassed mantle material^{7,9–14}. Here we perform numerical experiments of thermo-chemical convection to simulate the entrainment of primitive material by plumes generated at the top of primitive reservoirs in the deep mantle. We vary the chemical density contrast between the primitive, undegassed and regular, degassed mantle materials. We find that the simulations that reproduce the observed geometry of the heterogeneous regions also explain the geochemical signatures measured in ocean island basalts. In these simulations, the entrainment of primitive material into the mantle plume does not exceed 9%. We conclude that the presence of primitive reservoirs in the deep mantle is dynamically feasible and satisfies both seismological and geochemical constraints.

Increasing seismological evidence, mainly from seismic velocity ratios^{1–3} and from normal mode tomography^{4,5} indicates the existence of large-scale thermo-chemical heterogeneities in the lowermost (>2,000 km) mantle. The origin and nature of these chemical anomalies are still debated. Two endmember hypotheses, the subduction and segregation of mid-ocean-ridge basalt (MORB), and the survival of primitive reservoirs of dense material, are usually advocated. Subducted MORB is certainly contributing to the thermo-chemical structure of the deep mantle, but because it is seismically faster and denser than the average pyrolytic mantle it cannot explain alone all the features of global seismic tomography models, in particular the lack of correlation between density and shear-wave velocity anomalies (Supplementary Information). An additional deep reservoir of non-pyrolytic material is thus needed to fully explain seismological observations. The origin of this reservoir is probably related to early mantle differentiation^{6–8}, and its present shape and volume have probably been influenced by mantle convection.

Ocean island basalts (OIB) have specific isotopic signatures in rare gases (large scattering in ⁴He/³He ratio, large ⁴⁰Ar/³⁶Ar ratio) and trace elements (high ¹⁴³Nd/¹⁴⁴Nd) indicating that they originate from several reservoirs, one of which is undegassed^{7,9–14}. In OIB, ⁴He/³He ranges from 15,000 to 200,000, with large (>100,000) and low (<30,000) values being attributed to recycled crust and to a primitive reservoir, respectively^{9,10,12}. Thus, primitive reservoirs, if they exist, are not entirely isolated, but are partially sampled by OIB. The lowest value of ⁴He/³He observed in OIB, around 15,000 (ref. 13), imposes a constraint on the entrainment of

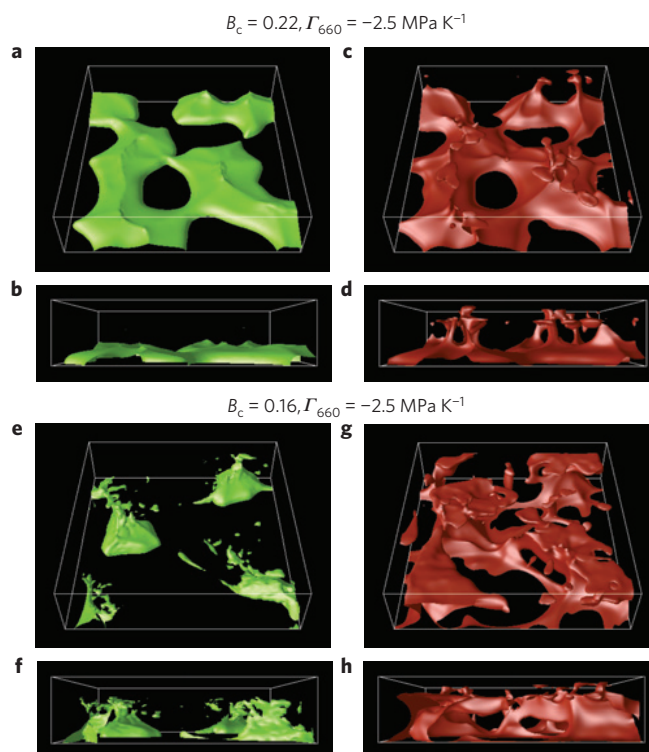


Figure 1 | Iso-surfaces of composition (left column) and residual temperature (right column) for two numerical experiments.

a–d, $B_c = 0.22$, and $\Gamma_{660} = -2.5 \text{ MPa K}^{-1}$. **e–h**, $B_c = 0.16$, and $\Gamma_{660} = -2.5 \text{ MPa K}^{-1}$. Residual temperature is defined as $T - T_m$, where T_m is the average temperature. Snapshots are taken at time $t = 6.3 \text{ Gyr}$. The isosurface value for the composition is $C = 0.5$ for both cases. The isosurface value of the temperature residue is $(T - T_m) = 0.085$ for the top case and $(T - T_m) = 0.070$ for the bottom case.

primitive material by plumes (Supplementary Information). For reasonable values (around 12,500) of ⁴He/³He in the primitive material ($[\text{}^4\text{He}/\text{}^3\text{He}]_{\text{PM}}$), the mass fraction of primitive material in plumes should not exceed 10% (ref. 15; Supplementary Fig. S2). Within the uncertainties in $[\text{}^4\text{He}/\text{}^3\text{He}]_{\text{PM}}$ this fraction may be larger, but shall never exceed 30%.

It has long been assumed that the primitive reservoir was the whole lower mantle^{9–12}, but the imaging of slabs penetrating in the deep mantle¹⁶ invalidated this hypothesis. This contradiction can be solved by assuming that the primitive reservoir is not the entire lower mantle, but consists of pools of chemically distinct material located in the lowermost mantle similar to those observed by seismology. Experimental and numerical models of thermo-chemical convection that include an initial basal layer of dense material

¹Institute of Geophysics, Swiss Federal Institute of Technology Zurich, 8092 Zurich, Switzerland, ²Institut de Physique du Globe, Sorbonne Paris Cité, Université Paris Diderot, UMR CNRS 7154, 75005 Paris, France. *e-mail: frederic@earth.sinica.edu.tw; deschamps@erdw.ethz.ch.

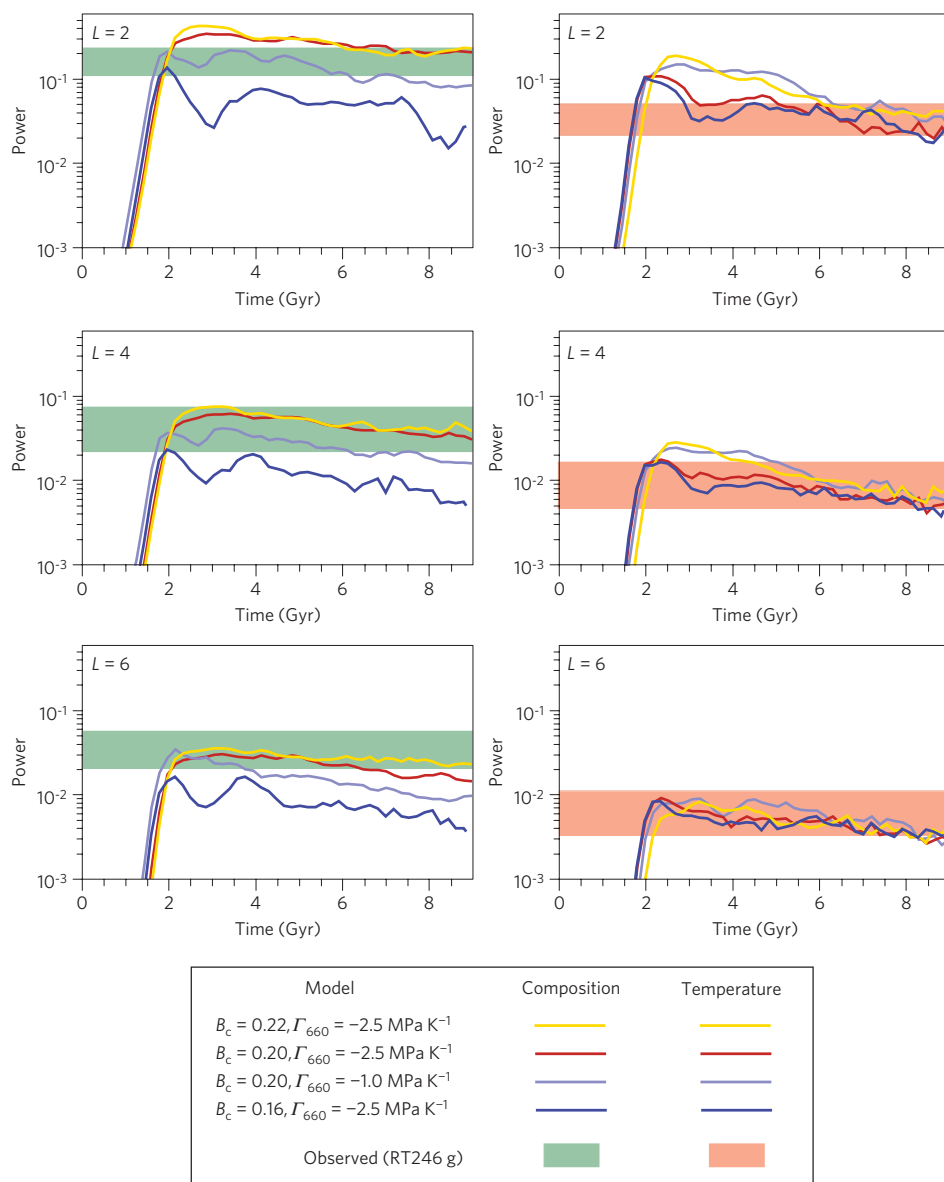


Figure 2 | Power spectra (spherical harmonic degrees $L = 2, 4$ and 6) of average chemical (left column) and thermal (right column) density anomalies in the lowermost layer ($2,000 \leq d \leq 2,891 \text{ km}$) for four models. $B_c = 0.22$ corresponds to stable pools and $B_c = 0.16$ corresponds to eroding piles. Fourier spectra of 3D-Cartesian thermo-chemical distributions are converted to spherical harmonic spectra (Supplementary Information). Resulting spectra are plotted as a function of time, and compared with those from probabilistic tomography (colour bands, covering two standard deviations around the average value)⁴.

showed that domes or pools with various topographies can be maintained at the bottom of the system for long periods of time^{17–26}. Two key parameters control the evolution of primitive reservoirs: the chemical density contrast between primitive and regular materials, and the thermal viscosity contrast. Maintaining primitive reservoirs in the deep mantle requires a moderate chemical density contrast (typically, around $80\text{--}100 \text{ kg m}^{-3}$), which avoids chemical stratification^{17–20,25}, and a strong thermal viscosity contrast, which avoids rapid mixing²⁴. Furthermore, the presence of an endothermic phase transition at 660-km depth prevents the primitive material from massively flowing to the upper mantle^{18,25,26}, thus influencing the entrainment of primitive material. In models combining these ingredients, pools of primitive material can be maintained during periods comparable to the age of the Earth. Interestingly, small plumes are generated at the top of these structures and reach the surface. Small amounts of primitive material

are entrained by plumes and are periodically injected into the upper mantle up to the surface, but this entrainment has not been quantitatively tested against the isotopic signature of OIB. Here, we use numerical models of thermo-chemical convection to quantify the entrainment of primitive material by plumes, and we show that this entrainment is consistent with OIB geochemical constraints.

We first performed a series of numerical experiments of thermo-chemical convection in 3D-Cartesian geometry (Supplementary Information), in which we varied the chemical buoyancy ratio (B_c , measuring the chemical density contrast between primitive and regular material) between 0.14 and 0.26 (that is, density contrasts between 60 and 110 kg m^{-3}), and the Clapeyron slope of the 660 km phase transition (Γ_{660}) between -3.0 and 0.0 MPa K^{-1} . These are conservative ranges for the Earth's mantle. As in previous models^{24,25}, we observe the formation of reservoirs of primitive material at the bottom of the system, and the generation of

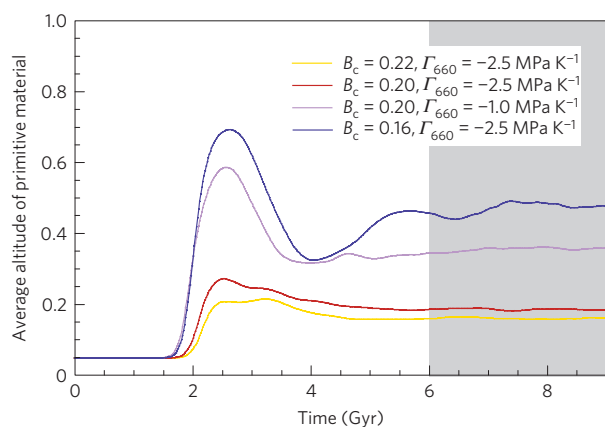


Figure 3 | Average altitude of primitive material (h_c) as a function of time for four cases. For convenience, the y-axis unit is scaled by the total thickness of the system D . The grey shaded band indicates the time range over which we averaged out the entrainment.

plumes at the top of these reservoirs. The shape and stability of the reservoirs vary strongly with B_c (Fig. 1) and, to a lesser extent, Γ_{660} . Time evolutions of the power spectra of chemical density anomaly distributions (Fig. 2) and of the average altitude of primitive material ($\langle h_c \rangle$, Fig. 3), provide quantitative estimates of the erosion rate of reservoirs (Supplementary Information). If primitive and regular materials are well mixed, $\langle h_c \rangle$ will be close to half the total thickness of the system (that is, $D/2$). In the case of chemical stratification, by contrast, $\langle h_c \rangle$ will remain constant at around half the initial thickness of the primitive layer (that is, $d_{\text{prim}}/2$, with $d_{\text{prim}} = 0.1D$ in all our calculations). For $B_c \geq 0.22$, large pools of primitive material with moderate topography (about 600–800 km) are generated at the bottom of the system whatever the value of Γ_{660} . These structures induce strong lateral anomalies in composition and temperature at the bottom of the system, as indicated by spectral heterogeneity maps and RMS profiles (Supplementary Figs S4 and S5, plots a,b), with power spectra consistent with those of probabilistic tomography⁴ (Fig. 2). Pools are slightly eroded (plumes entrain some material upwards), but the value of $\langle h_c \rangle$ by the end of the run is nearly constant around $0.15D$ (Fig. 3), indicating that the erosion rate is small. Pools are thus maintained over periods of time longer than the age of the Earth. By contrast, for $B_c \leq 0.16$, medium size piles with larger topography (around 1,200 km) are generated, inducing moderate thermo-chemical anomalies at the bottom of the system (Supplementary Figs S4 and S5, plots g,h). More importantly, the erosion rate of these piles is much larger than that of the pools. In the long term, the compositional density anomalies do not explain probabilistic tomography (Fig. 2), and $\langle h_c \rangle$ is close to $0.5D$ (Fig. 3), indicating that primitive and regular materials are well mixed. For intermediate values of B_c , we again observe the formation of pools with moderate topography, but whether these pools are maintained for a long period of time or are eroded depends on the value of Γ_{660} (Figs 2 and 3). The endothermic phase transition at 660 km induces negative buoyancy that adds to the chemical buoyancy, thus opposing the penetration of primitive material above the phase transition. As an example, for $B_c = 0.2$ the transition from a stable to an eroding pool occurs for a value of Γ_{660} between -1.5 and -1.0 MPa K⁻¹.

Plumes rising from the top of the pools entrain a small amount of primitive material upwards. The resolution of our models allows this entrainment to be measured with sufficient accuracy (Supplementary Information). The amount of entrained material

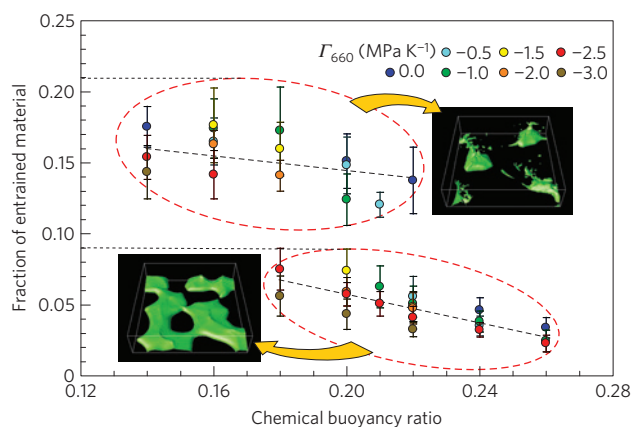


Figure 4 | Entrainment of primitive material, defined as the fraction x_{PM} of primitive material in plumes. Results are presented as a function of B_c (horizontal axis) and of Γ_{660} (colour code). The circles and error bars represent the time-averaged and standard deviation in x_{PM} over a period of time covering the last third of the run (equivalent to 3.0 Gyr).

strongly depends on the dynamics of the system. We estimated the extent of plumes by defining threshold values for the plume temperature²⁷ (Supplementary Information) and calculated the mass fraction x_{PM} of primitive material in these plumes (with respect to the total plumes' mass) above the phase transition (Supplementary Information). Our experiments indicate that both B_c and, to a lesser extent, Γ_{660} have an influence on x_{PM} (Fig. 4). For $B_c \geq 0.22$, the entrainment of primitive material is small ($x_{\text{PM}} < 7\%$ within error bars) whatever the value of Γ_{660} we considered (except for $\Gamma_{660} = 0$). For $B_c \leq 0.16$, by contrast, we observed significant entrainment ($x_{\text{PM}} > 11\%$ within error bars) for all the values of Γ_{660} we considered. For intermediate values of B_c , the endothermic phase transition, which increases the negative buoyancy of the primitive material, plays a role in controlling the entrainment of this material. If Γ_{660} is sufficiently negative, the upwards flow of primitive material across the phase transition is reduced, and x_{PM} remains below 10% (Fig. 4). Overall, our calculations are thus distributed in two groups, one corresponding to stable pools with values of x_{PM} smaller than 10%, and the other to eroding piles and pools with values of x_{PM} larger than 10%. Because they fit probabilistic tomography better in the long term, stable pools seem more likely thermo-chemical structures for the bottom mantle than eroding piles. These models also correspond to the most likely values of B_c (between 0.20 and 0.22) and Γ_{660} (between -3.0 and -2.0 MPa K⁻¹). For these models, the fraction of primitive material in plumes is always lower than 9% (Fig. 4). When accounting for the less likely eroding piles models, the fraction of primitive material in plumes remains lower than 21%, still an acceptable value if $[\text{}^4\text{He}/\text{}^3\text{He}]_{\text{PM}}$ is high (around 13,500; Supplementary Fig. S2).

Further experiments (Supplementary Information) indicate that entrainment is sensitive to the thermal viscosity contrast. Because the contrast we imposed in our experiments corresponds to a conservative value of the activation energy (which controls the amplitude of thermal viscosity variations), the entrainments we estimated may be taken as upper bounds of the entrainment in plumes. Variations of the thermal expansion α with pressure and temperature also influence the dynamics of primitive reservoirs. The decrease of α with pressure is accounted for in our models, and favours the stability of primitive reservoirs, even if the buoyancy ratio is defined relative to the surface α . By contrast, thermal variations of α , which are not included in our models, may decrease the stability of primitive reservoirs. This effect can however be balanced by slightly increasing the buoyancy ratio (see Supplementary Information).

As they predict entrainments that are quantitatively consistent with OIB data, our numerical experiments support the hypothesis that OIB partially sample a dynamically stable reservoir of primitive material buried in the deep mantle. This reservoir is not the lower mantle itself, but rather consists of discontinuous pools with topography of several hundreds of kilometres. Plumes are generated at the top of these pools and entrain small amounts of primitive material that do not exceed the value predicted by the lowest values of the $^4\text{He}/^3\text{He}$ observed in OIB. These conclusions are not affected by the exact nature and origin of the primitive pools, which are still a matter of debate. A possibility is that primitive reservoirs are enriched in iron and silicate by a few per cent, as suggested by probabilistic tomography⁴, geochemical data²⁸, and recent enstatite chondrite models of Earth composition²⁹. Because it may reach the bottom of the mantle, interact with the primitive pools, and be partly entrained by rising plumes, recycled MORB should also be accounted for in future models and calculations. Incorporating, simultaneously, primordial and recycled sources of chemical heterogeneities will refine the interpretation of key geochemical and geophysical observables, including the high ($>100,000$) $^4\text{He}/^3\text{He}$ in OIB, and the lack of correlation between shear-wave velocity and density anomalies.

Received 27 February 2011; accepted 15 September 2011;
published online 23 October 2011

References

- van der Hilst, R. D. & Káráson, H. Compositional heterogeneities in the bottom 1,000 km of Earth's mantle: Towards a hybrid convection model. *Science* **283**, 1885–1888 (1999).
- Masters, G., Laske, G., Bolton, H. & Dziewonski, A. M. in *Earth's Deep Interior: Mineral Physics and Tomography from the Atomic to the Global Scale* (eds Karato, S.-I. *et al.*) 63–87 (Geophysical Monograph Ser., Vol. 117, American Geophysical Union, 2000).
- Deschamps, F. & Trampert, J. Mantle tomography and its relation to temperature and composition. *Phys. Earth Planet. Inter.* **140**, 277–291 (2003).
- Ishii, M. & Tromp, J. Normal-mode and free-air gravity constraints on lateral variations in velocity and density of Earth's mantle. *Science* **285**, 1231–1236 (1999).
- Trampert, J., Deschamps, F., Resovsky, J. S. & Yuen, D. A. Probabilistic tomography maps significant chemical heterogeneities in the lower mantle. *Science* **306**, 853–856 (2004).
- Solomatov, V. S. & Stevenson, D. J. Suspension in convective layers and style of differentiation of a terrestrial magma ocean. *J. Geophys. Res.* **98**, 5375–5390 (1993).
- Boyett, M. & Carlson, R. W. ^{142}Nd evidence for early (>4.53 Ga) global differentiation of the silicate Earth. *Science* **309**, 576–581 (2005).
- Lee, C.-T. *et al.* Upside-down differentiation and generation of a 'primordial' lower mantle. *Nature* **463**, 930–933 (2010).
- Allègre, C. J., Staudacher, T., Sarda, P. & Kurtz, M. Constraints on evolution of Earth's mantle from gas rare systematic. *Nature* **303**, 762–766 (1983).
- Farley, K. A., Natland, J. H. & Craig, H. Binary mixing of enriched and undegassed (primitive?) mantle components (He, Sr, Nd, Pb) in Samoan lavas. *Earth Planet. Sci. Lett.* **111**, 183–199 (1992).
- Allègre, C. J., Hofmann, A. & O'Nions, K. The Argon constraints on mantle structure. *Geophys. Res. Lett.* **24**, 3555–3557 (1996).
- Hofmann, A. W. Mantle geochemistry: The message from oceanic volcanism. *Nature* **385**, 219–229 (1997).
- Stuart, F. M., Lass-Evans, S., Fitton, J. G. & Ellam, R. M. High $^3\text{He}/^4\text{He}$ ratios in picritic basalts from Baffin Island and the role of a mixed reservoir in mantle plumes. *Nature* **424**, 57–59 (2003).
- Jackson, M. G. *et al.* Evidence for the survival of the oldest terrestrial mantle reservoir. *Nature* **466**, 853–856 (2010).
- Allègre, C. J. & Moreira, M. Rare gas systematic and the origin of oceanic islands: The key role of entrainment at the 670 km boundary layer. *Earth Planet. Sci. Lett.* **228**, 85–92 (2004).
- van der Hilst, R. D., Widiyantoro, S. & Engdahl, E. R. Evidence for deep mantle circulation from seismic tomography. *Nature* **386**, 578–584 (1997).
- Davaille, A. Simultaneous generation of hotspots and superswells by convection in a heterogeneous planetary mantle. *Nature* **402**, 756–760 (1999).
- Le Bars, M. & Davaille, A. Whole layer convection in a homogeneous planetary mantle. *J. Geophys. Res.* **109**, B03403 (2004).
- Tackley, P. J. Strong heterogeneity caused by deep mantle layering. *Geochem. Geophys. Geosyst.* **3**, 1024 (2002).
- McNamara, A. K. & Zhong, S. Thermochemical structures within a spherical mantle. *J. Geophys. Res.* **109**, B07402 (2004).
- McNamara, A. K. & Zhong, S. Thermochemical structure beneath Africa and the Pacific ocean. *Nature* **437**, 1136–1139 (2005).
- Tan, E. & Gurnis, M. Metastable superplumes and mantle compressibility. *Geophys. Res. Lett.* **32**, L20307 (2005).
- Tan, E. & Gurnis, M. Compressible thermo-chemical convection and application to the lower mantle. *J. Geophys. Res.* **112**, B06304 (2007).
- Deschamps, F. & Tackley, P. J. Exploring the model space of thermo-chemical convection I—principles and influence of the rheological parameters. *Phys. Earth Planet. Inter.* **171**, 357–373 (2008).
- Deschamps, F. & Tackley, P. J. Exploring the model space of thermo-chemical convection II—influence of physical and compositional parameters. *Phys. Earth Planet. Inter.* **176**, 1–18 (2009).
- van Summeren, J. R. G., van den Berg, A. P. & van der Hilst, R. D. Upwellings from a deep mantle reservoir filtered at the 660 km phase transition in thermo-chemical convection models and implications for intra-plate volcanism. *Phys. Earth Planet. Inter.* **172**, 210–224 (2009).
- Labrosse, S. Hotspots, mantle plumes and core heat loss. *Earth Planet. Sci. Lett.* **199**, 147–156 (2002).
- Humayun, M., Qin, L. & Norman, N. D. Geochemical evidence for excess iron in the mantle beneath Hawaii. *Science* **306**, 91–94 (2004).
- Javoy, M. *et al.* The chemical composition of the Earth: Enstatite chondrite model. *Earth Planet. Sci. Lett.* **293**, 259–268 (2010).

Acknowledgements

We are grateful to A. McNamara and A. van den Berg for their useful and constructive comments and reviews. All thermo-chemical models of convection were calculated on ETH super-cluster Brutus.

Author contributions

All three authors equally contributed to the project.

Additional information

The authors declare no competing financial interests. Supplementary information accompanies this paper on www.nature.com/naturegeoscience. Reprints and permissions information is available online at <http://www.nature.com/reprints>. Correspondence and requests for materials should be addressed to F.D.